

Article

Influence of Continuous Annealing Temperature on Mechanical Properties and Texture of Battery Shell Steel

Beijia Ning^{1,2}, Zhengzhi Zhao^{1,2,*} , Zhiying Mo^{1,2}, Hong Wu³, Chong Peng³ and Honggen Gong³

¹ Collaborative Innovation Center of Steel Technology, University of Science and Technology Beijing, Beijing 100083, China; 17888803573@163.com (B.N.); mzyeric@163.com (Z.M.)

² Beijing Laboratory for Modern Transportation Advanced Metal Materials and Processing Technology, University of Science and Technology Beijing, Beijing 100083, China

³ Xinyu Iron Steel Group Co., Ltd., Xinyu 338001, China; wuhong36@126.com (H.W.); 019pen@xinsteel.com.cn (C.P.); ghg@xinsteel.com.cn (H.G.)

* Correspondence: zhaozhzhi@ustb.edu.cn; Tel.: +86-10-6233-2617

Received: 25 November 2019; Accepted: 11 December 2019; Published: 27 December 2019



Abstract: To study the influences of continuous annealing temperature on microstructure, mechanical properties and textures of battery shell steel, continuous annealing experiments were conducted at 710 °C, 730 °C, 760 °C and 780 °C respectively. The mechanical properties and normal anisotropy index (r) were measured by tensile test and the textures were investigated using the method of electron backscatter diffraction (EBSD). The results show that as annealing temperature rose, the grain size, fracture elongation and r value increased, whereas the strength and yield ratio decreased. The yield strength was 122 MPa, the tensile strength was 286 MPa, meanwhile the elongation and r value arrived at 38.8% and 2.3 when the annealing temperature rose to 780 °C. After annealing, the main texture in battery shell steel is $\{111\} \langle 112 \rangle$, followed by $\{111\} \langle 110 \rangle$. With the increase of annealing temperature, textures in $\{001\}$ crystallographic plane weakened while textures in $\{111\}$ plane strengthened, which is beneficial to the deep drawability of the steel.

Keywords: battery shell steel; annealing temperature; mechanical properties; crystallographic texture

1. Introduction

In recent years, as the sustainable development concept of energy-saving and environment protection gets popular, new energy vehicles have been developed rapidly. The battery shell steel used to produce the shell of battery pack, which is the core component of new energy automobiles, has received extensive attention at the same time [1]. As a kind of precise cold-rolled steel sheet, the battery shell steel has high technology content and high-quality requirements. The thickness of sheet used commonly is 0.25–0.50 mm, and the surface quality is required to reach “05” level in both sides [2,3], thus bringing great difficulties to production. During the process of forming, the steel needs to go through deep drawing and ironing for more than one time. All processes go on automatically with high speed but many problems exist in them, such as blocking in the mold, fracture, earing, etc. [4]. These problems have a direct connection with deep drawability of the steel, which is influenced by many factors including strengthening mechanisms, grain size, morphology and orientation. All these micro factors are affected by the annealing process directly and significantly.

Strain hardening and internal stress occur in cold rolling, making the steel become hard and brittle. To recover the ductility and increase the formability, annealing treatment is required. Normal anisotropy index (r) is an important factor for optimizing deep drawability. The value of r can be

increased with a strong γ fiber (ND//<111>), and weak α (RD//<110>) and θ (ND//<100>) fibers [5,6]. Though a certain texture may have benefits on deep drawability for one particular deformation state, it may result in poor properties for another. For battery shell steel under the ideal plain-strain condition, a better deep drawability can be obtained when there are strong {111} textures. By optimizing the parameters of the annealing process, the density of {111} texture and r value can be increased, thus improving the drawability [7–9].

For battery shell steel, a lot of studies on surface defects and experiments on formability characterization have been done. However, there is not enough attention put on the annealing process, which can optimize the formability and avoid the defects primarily as mentioned. In the present study, effects of annealing temperature on microstructures, mechanical properties, component of textures were investigated based on optical microscope (OM), electron backscatter diffraction (EBSD) and tensile test. Moreover, the anisotropy of the annealed steel was paid attention to, especially the relationship between r values and typical textures. Combining all the results, the suitable annealing temperature is aimed to be put out to obtain stronger favorable textures in order to achieve a higher r value and better drawability of the annealed sheet. Since the property of battery shell steel is improved, larger competitiveness of some steel mills can be realized and more contribution can be made to the development of new energy automobiles.

2. Materials and Methods

The material used for the experiment is a kind of cold-rolled steel sheet with a thickness of 0.3 mm from a commercial steel company. The grade of the experimental steel is XDCK and the chemical composition is shown in Table 1.

Table 1. Chemical composition of the tested steel (mass fraction, %).

C	Si	Mn	S	P	Al	Ti	N
≤0.010	≤0.300	0.100–0.500	≤0.010	≤0.015	0.010–0.070	0.010–0.050	≤0.003

Specimens with the dimension of 70 mm × 220 mm were cut from the cold-rolled sheet and then continuous annealing tests were carried out using CCT-AY-II (made by ULVAC, Tokyo, Japan). In different annealing tests, specimens were heated to the soaking temperatures of 710 °C, 730 °C, 760 °C and 780 °C respectively with a hold of 80 s. After a short slow cooling, they were continuously cooled rapidly to about 400 °C for over aging treatment and finally cooled to room temperature.

For tensile tests, samples with a gauge length of 50 mm and a gauge width of 12.5 mm according to standard GB/T 228.1-2010 were cut along the directions of 0°, 45° and 90° to rolling direction respectively and directly from each annealed sheet. Then tensile tests were conducted at room temperature with a constant speed (2 mm/min). The r values in each direction were measured in accordance with standard GB/T 5027-2016 and the Δr value was calculated by:

$$\Delta r = (r_0 - 2r_{45} + r_{90})/2, \quad (1)$$

where r_0 , r_{45} and r_{90} represent the r values in three directions (0°, 45° and 90°). For the same direction on the same annealed sheet, three samples were tested and the results were averaged.

The microstructures of the cold rolled sheet and annealed samples were observed by OLS4100 (made by OLYMPUS, Tokyo, Japan). The samples for EBSD were cut perpendicular to the rolling direction and were electrolytically polished with a solution containing 10 vol% perchloric and 90 vol% ethanol. The polishing process was carried out using a DC power supply for 10–20 s at 15 V and 1 A.

3. Results and Discussion

3.1. Microstructure of the Annealed Sheet

It can be seen in Figure 1a that the cold rolling morphology of the tested material is a kind of fibrous structure elongated along rolling direction. The microstructures of the samples annealed at different temperatures are shown in Figure 1b–e. In all four samples, only ferrite phase existed. Compared with the microstructure of cold rolled sheet, recrystallization happened at all annealing temperatures. Besides, the grains were still elongated along the rolling direction to a certain extent as the shape of pie. With the rise of the annealing temperature, the recrystallization was more complete, and the proportion of equiaxed grains was further increased. Using the EBSD method and Oxford software, hundreds of grains' sizes were counted and then the grain size distribution at different annealing temperatures can be obtained (Figure 2). When the annealing temperature was 710 °C the size of grains with the largest proportion was around 5.6 μm . As the temperature rose to 730 °C and 760 °C the proportions of the grains having a diameter of 7.9 μm and 11.2 μm increased. At 780 °C more grains reached the size of 11.2 μm and 15.9 μm . The average grain size can also be given according to the results of EBSD, which is marked particularly in Figure 2. Combining the analyses of Figures 2 and 3, we could say that the higher the annealing temperature is, the greater the crystallization degree is, and the larger the grain size is.

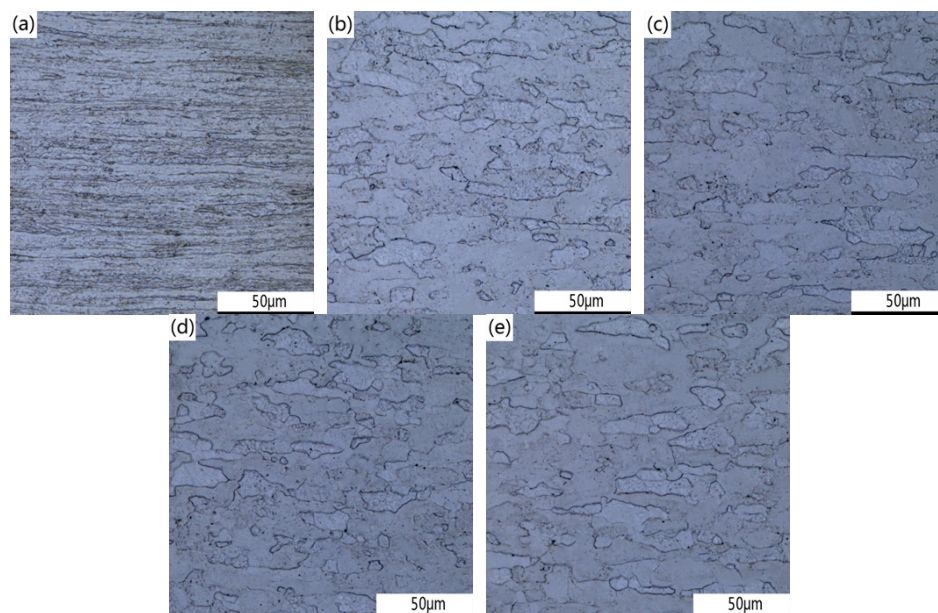


Figure 1. Microstructures of tested steel. (a) Cold rolled sample and (b–e) annealed samples at 710 °C, 730 °C, 760 °C and 780 °C respectively.

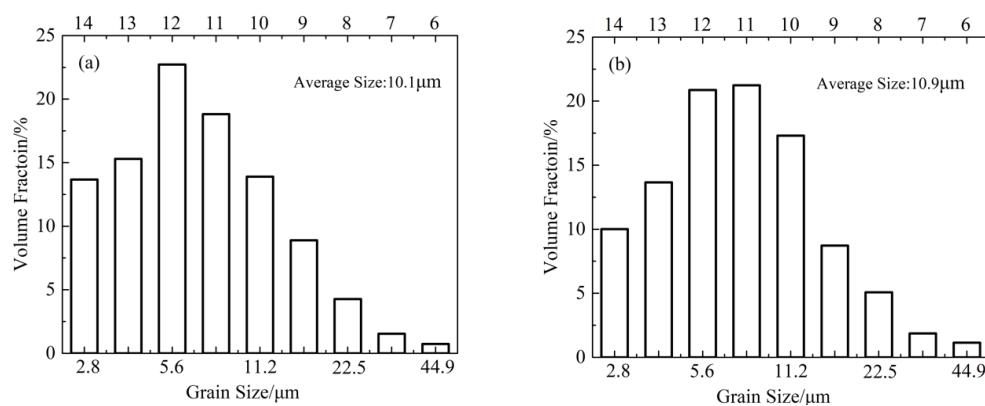


Figure 2. Cont.

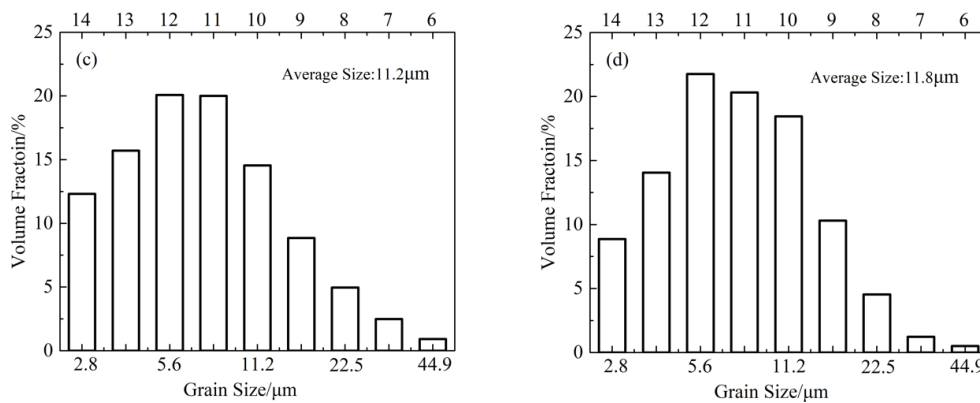


Figure 2. Grain size distribution at different annealing temperatures. (a) 710 °C, (b) 730 °C, (c) 760 °C and (d) 780 °C.

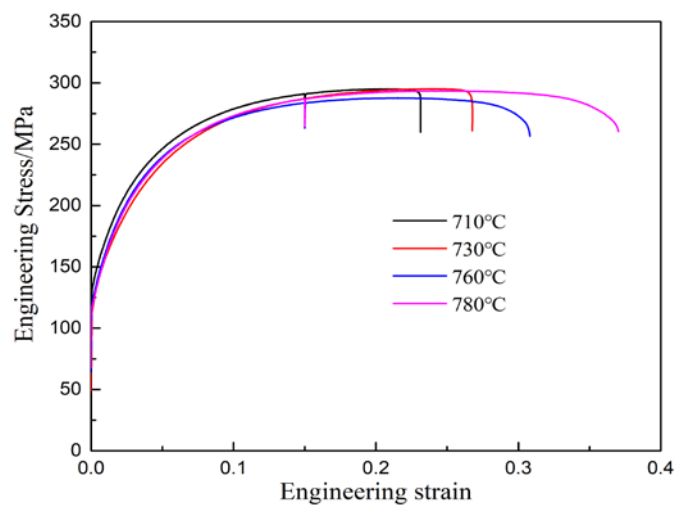


Figure 3. Engineering stress–strain curves at different annealing temperatures perpendicular to the rolling direction.

3.2. Mechanical Properties

Figure 3 shows the engineering stress–strain curve of samples annealed at different temperatures obtained from one of the three repetitive tensile tests. Figure 4a shows the effect of annealing temperature on yield strength, tensile strength, yield ratio and fracture elongation. With the increase of annealing temperature, the yield strength, tensile strength and the yield ratio decreased generally, while the fracture elongation showed an upward trend. As the annealing temperature rose from 730 to 780 °C, the yield strength decreased from 140 to 122 MPa, the tensile strength decreased from 300 to 286 MPa, and the elongation increased from 29.7% to 38.8%. When annealing at lower temperature, the incomplete recrystallization degree and the residual stress of cold rolling lead to high yield strength. When the temperature rises, the driving force of recrystallization increases, thus causing the development of grain size. The grain boundary area reduces due to grain coarsening and the residual stress eliminates due to temperature increasement. All these factors have something to do with the decrease of yield and tensile strength and the increase of elongation. However, when the temperature reached 780 °C the recrystallization was gradually completed, and the influence of residual stress in cold rolling was gradually eliminated. At this time, the influence of annealing temperature on strength was weakened.

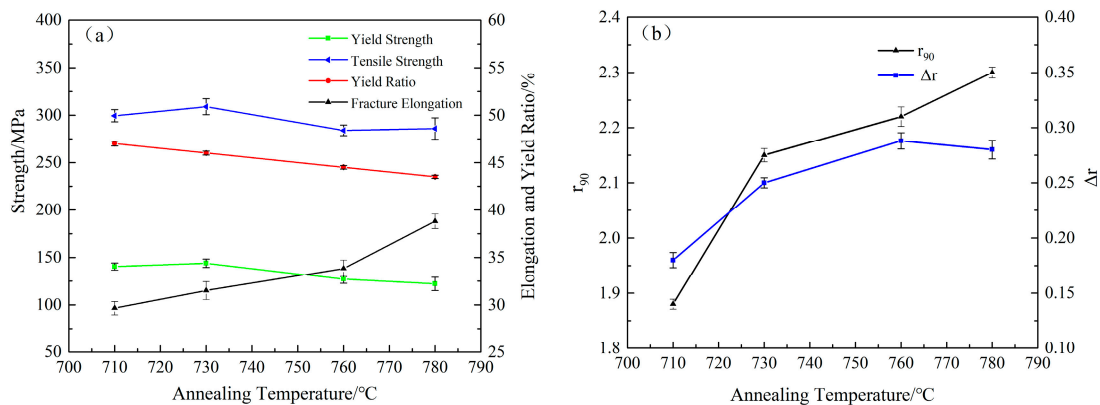


Figure 4. Effects of annealing temperature on mechanical properties. (a) Strength, elongation and yield ratio perpendicular to the rolling direction and (b) r_{90} and Δr .

Figure 4b reflects the effect of annealing temperature on the values of normal anisotropy (r) and planar anisotropy coefficient (Δr). As the annealing temperature rose, r_{90} increased, which is beneficial to deep drawability of the steel. However, the Δr value also showed an increasing trend except for a minor decrease at 780 °C. This indicates that the difference among the three directions gets larger with the increase of annealing temperature.

3.3. Texture Analysis by EBSD

The texture results of annealed specimens are illustrated in Figure 5 in the form of orientation distribution function (ODF) sections with $\varphi_2 = 45^\circ$. In all cases, the textures were mainly made up of fine γ fibers with $\langle 111 \rangle$ parallel to the normal direction. To make the results more visualized, density distributions of the textures on α (a) and γ (b) orientation lines are presented in Figure 6. It can be seen in Figure 6a that the strongest components belonging to α fibers were all close to $\{112\} \langle 110 \rangle$ and $\{111\} \langle 110 \rangle$ at different annealing temperatures. Besides the overall strength of α fibers in the sample annealed at 710 °C was high. This is because the driving force of recrystallization is weak and part of γ fibers formed in the process of cold rolling remains at low annealing temperature. The α fibers are characterized by a $\langle 110 \rangle$ crystal direction perpendicular to the rolled surface of the steel plate, making the deformation resistance weak and the deep drawability of the steel sheet poor. However, with the increase of annealing temperature, the strength of α fibers decreased as a whole, and the $\{111\} \langle 110 \rangle$ component gradually became the sharpest texture. Especially at 730 °C, α fibers almost disappeared except for those close to $\{111\} \langle 110 \rangle$.

Figure 6b indicates that the average texture density on γ orientation line increased with the rise of annealing temperature. The density of $\{111\} \langle 112 \rangle$ had the largest increasement, from 8.4 at 710 °C to 13.8 at 780 °C. The strength of γ fiber is closely related to the stored energy of cold rolling textures. The textures formed in the cold-rolled process mainly contain $\{111\} \langle 112 \rangle$, $\{111\} \langle 110 \rangle$, $\{112\} \langle 110 \rangle$ and $\{100\} \langle 110 \rangle$ components. The stored energy in different textures is different, and the order is as follows [10,11]:

$$E_{\{110\} \langle 001 \rangle} < E_{\{001\} \langle 110 \rangle} < E_{\{112\} \langle UVW \rangle} < E_{\{111\} \langle UVW \rangle} < E_{\{110\} \langle 110 \rangle}.$$

The higher the stored energy is, the more likely for the process of recovery and recrystallization to happen. As we have mentioned, the grain size gets larger when the annealing temperature is higher. Bigger grains with the orientation of $\{111\}$ tend to grow preferentially by merging other small grains. That is the reason why γ fibers owned a high density. Moreover, researches show that preferred nucleation promotes the formation of $\{111\} \langle 110 \rangle$ texture, while preferred growth promotes the formation of $\{111\} \langle 112 \rangle$ texture [12]. The $\{111\} \langle 112 \rangle$ texture is much stronger than $\{111\} \langle 110 \rangle$ texture at the same annealing temperature. However, they were almost the same at 710 °C. At this

time, the uniformity of γ fibers was better, which is conducive to reducing the earing of battery shell steel in the stamping process. Besides, as the annealing temperature rose, some $\{111\} \langle 110 \rangle$ and $\{111\} \langle 112 \rangle$ grains began to nucleate inside each other. However, the nucleation rate of $\{111\} \langle 110 \rangle$ grains was higher than that of $\{111\} \langle 112 \rangle$ grains. Though $\{111\} \langle 112 \rangle$ owned the crystal nucleus with the maximum grain boundary migration rate, the low nucleation rate still resulted in the weaker density in 760 °C than 730 °C. On the other side, in a certain range of temperatures, the interstitial atoms are fixed and the solid solution of substitutional solute atoms increases as temperature rises, which hinder the dislocation movement and reduce the effective deformation, thus providing conditions for the preferred growth of $\{111\} \langle 112 \rangle$ texture. Therefore, when the annealing temperature increased, the difference of density between the two textures became more obvious.

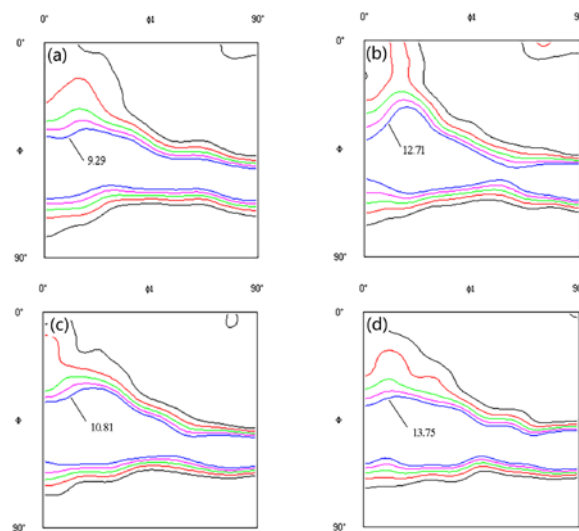


Figure 5. Orientation distribution function (ODF) sections ($\varphi_2 = 45^\circ$) at different annealing temperatures. (a) 710 °C, (b) 730 °C, (c) 760 °C and (d) 780 °C.

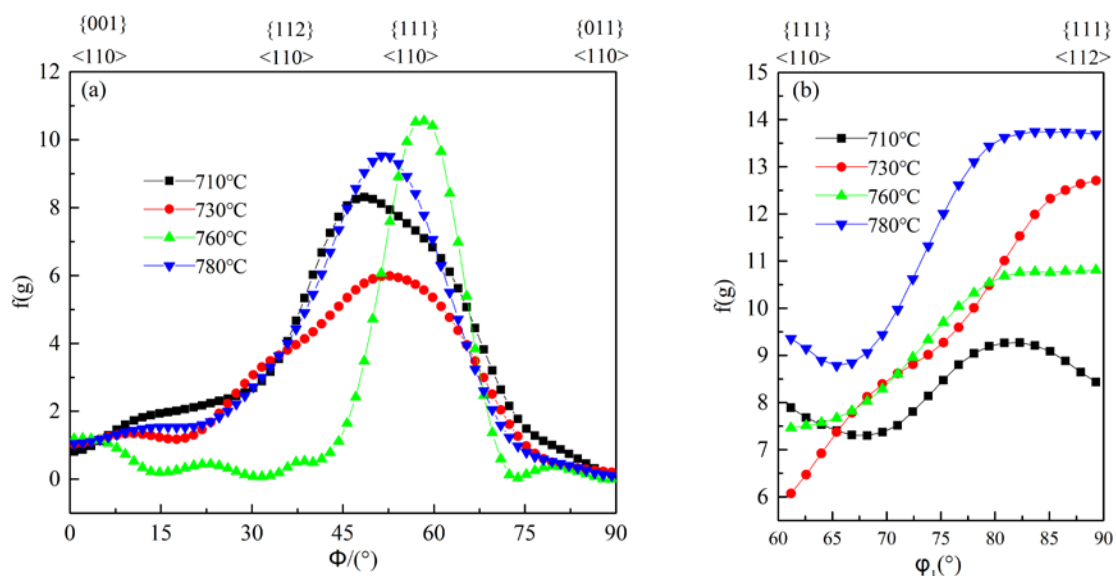


Figure 6. Texture intensity distributions along α (a) and γ (b) orientation lines at different annealing temperatures.

It is known that EBSD is a useful tool to observe microstructural textures, grain orientations, grain boundaries, etc. Figure 7 shows the distribution maps of several typical textures in specimens annealed at different temperatures and the volume fraction of each texture is shown in Table 2. The increase

of grain size and the decrease of elongation along the rolling direction with the rise of annealing temperature can also be seen in Figure 7. Besides, Figure 7 and Table 2 give us a clear recognition that the main textures in the annealed sheets are $\{111\} \langle 112 \rangle$ components, followed by $\{111\} \langle 110 \rangle$ and $\{112\} \langle 110 \rangle$ components. Taylor factor (M) is often used to represent the effect of textures on yield strength. The M-value of rolling textures is usually 15% higher than that of annealing textures [13]. With the annealing temperature rising, the volume fractions of $\{111\} \langle 112 \rangle$, $\{111\} \langle 110 \rangle$ and other annealing textures increased, thus resulting in the decrease of yield strength, which is one of the results of the tensile test.

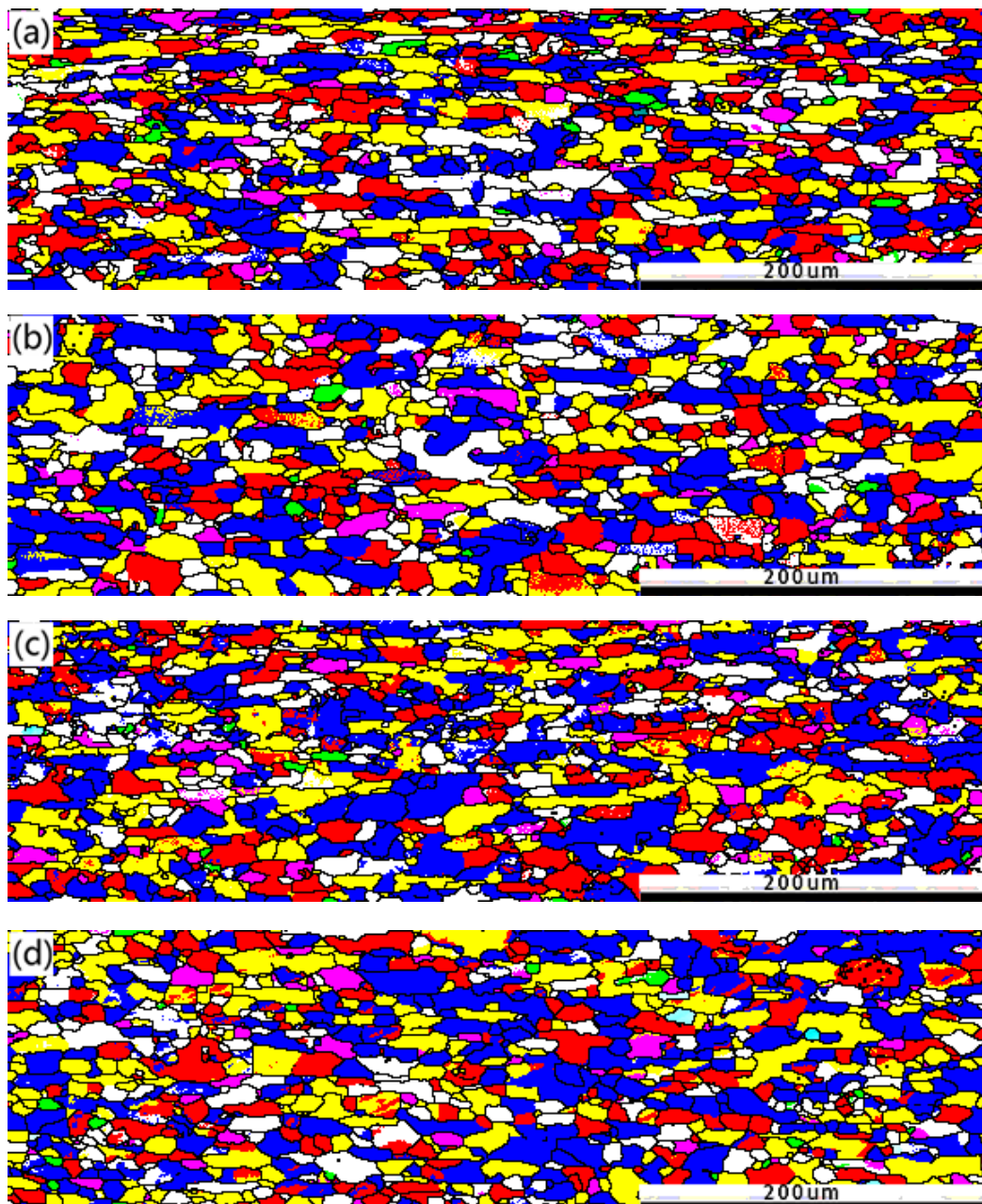


Figure 7. Distribution maps of typical textures at different annealing temperatures. (a) 710 °C, (b) 730 °C, (c) 760 °C and (d) 780 °C. Blue represents $\{111\} \langle 112 \rangle$ texture, red represents $\{111\} \langle 110 \rangle$, yellow represents $\{112\} \langle 110 \rangle$, purple represents $\{001\} \langle 110 \rangle$ and green represents $\{001\} \langle 001 \rangle$.

Table 2. Volume fractions of typical textures at different annealing temperatures.

Annealing Temperature/°C	{111} <112>/%	{111} <110>/%	{112} <110>/%	{001} <110>/%	{001} <001>/%	{111}/%	{001}/%	{111}/{001}
710	42.30	33.00	22.20	5.15	1.07	68.80	11.00	6.25
730	44.11	29.80	24.20	4.91	0.87	69.80	9.41	7.42
760	44.00	32.40	24.30	4.11	1.79	70.30	9.55	7.36
780	46.30	33.20	26.00	4.55	1.34	73.40	8.92	8.23

The effect of textures on anisotropy is realized by the influence of Taylor factor on yield locus, which means that anisotropy can be judged by the volume fraction and M-value of the textures. {100} textures have the lowest M-value at the same condition. Therefore, plastic flow behavior is more likely to happen along the <001> direction during the process of deep drawing, thus causing the appearance of earing [14,15]. Researches have shown that r value has a linear relationship with the volume ratio of {111} textures to {100} textures [16,17], which is presented as {111}/{100} in Table 2. It can be seen that the value of {111}/{100} increased as the annealing temperature rose, which is beneficial for the improvement of r value and deep drawability. This observation is just in keeping with the rising trend of r values as shown in Figure 4b.

4. Conclusions

1. In the continuous annealing process of battery shell steel, with the increase of annealing temperature, the recrystallization of ferrite phase was more complete and the average grain size was larger. Besides, both yield strength and tensile strength decreased, while the fracture elongation and r value increased.
2. The annealed sheets contained strong γ fibers and weak α fibers. The density of {111} <112> texture was the highest, followed by {111} <110> and {112} <110> textures. Besides the content of {001} texture was extremely low.
3. As annealing temperature rose, the volume fraction of {111} textures increased, while volume fraction of {001} textures decreased, causing a higher value of {111}/{001}, which is an important factor affecting the r value and the deep drawability.

Author Contributions: Conceptualization, B.N. and Z.Z.; methodology, B.N. and Z.M.; validation, H.W. and H.G.; formal analysis, Z.Z., B.N. and C.P.; writing—original draft preparation, B.N.; writing—review and editing, Z.M. and C.P.; supervision, H.W.; project administration, Z.Z. All authors have read and agreed to the published version of the manuscript.

Funding: This research received no external funding.

Conflicts of Interest: The authors declare no conflict of interest.

References

1. Zhao, H.-B.; Li, M.-L.; Li, M.-Y. Research progress and application situation of steel for battery box of battery electric vehicles. *Hebei Metal*. **2016**, *9*, 1–4.
2. Wang, X.-H. Non-metallic inclusion control technology for high quality cold rolled steel sheets. *J. Iron Steel* **2013**, *48*, 1–7.
3. Asensio, J.; Romano, G.; Martinez, V.J.; Verdeja, J.I.; Pero-Sanz, J.A. Ferritic steels optimization of hot-rolled textures through cold rolling and annealing. *Mater. Charact.* **2001**, *47*, 119–127. [[CrossRef](#)]
4. Xue, F.; Liu, J.-L.; Ji, S.-K.; Fan, Y.-H. Discussion on typical surface defects of battery shell and their causes. *Baosteel Tech.* **2014**, *5*, 67–75.
5. černík, M.; Gburik, R.; Hrabčáková, L.; Vranec, P. Texture analysis of tinplate steel and its application in production of double reduced high strength tinplate grades with controlled earing properties. *Mater. Sci. Eng.* **2015**, *82*, 012108.
6. Zhao, H.; Rama, S.C.; Barber, G.C.; Wang, Z.; Wang, X. Experimental study of deep drawability of hot rolled IF steel. *J. Mater. Process. Technol.* **2002**, *128*, 73–79. [[CrossRef](#)]

7. Pasi, J.; Dierk, R.; Pentti, K.; Tero, K.; Gerd, B. Optimizing continuous annealing of Interstitial-Free steels for improving deep drawability. *Metall. Mater. Trans. A* **2001**, *32*, 1989–1995.
8. He, T.; Liu, Y.-D.; Sun, W.; Zuo, L. Formation of nuclei with {111}<110> and {111}<112> orientations of IF steel at early stage of recrystallization using EBSD analysis. *J. Iron Steel Res. Int.* **2012**, *20*, 61–66. [[CrossRef](#)]
9. Hirotsuke, I. Fundamental aspect of texture formation in low carbon steel. *ISIJ Int.* **1994**, *34*, 313–321.
10. Wauthier, A.; Chauveau, T.; Castelnau, O.; Réglé, H.; Bacroix, B. The evolution with strain of the stored energy in different texture components of cold-rolled IF steel revealed by high resolution X-ray diffraction. *Mater. Charact.* **2015**, *104*, 31–41. [[CrossRef](#)]
11. Wierzbowski, K.; Baczmanński, A.; Tarasiuk, J.; Lipinski, P.; Bacroix, B.; Lodin, A. Stored energy and recrystallization in cold rolled steel. *Mater. Sci. Forum* **2007**, *558*, 1207–1212. [[CrossRef](#)]
12. Yang, P.; Li, Z.-C.; Mao, W.-M.; Zhao, Z.-S. Formation of the {111}<112> annealing texture in steels. *Trans. Mater. Heat Treat.* **2009**, *30*, 46–52.
13. Starink, M.J.; Wang, S.C. A model for the yield strength of overaged Al–Zn–Mg–Cu alloys. *Acta Mater.* **2003**, *51*, 5131–5150. [[CrossRef](#)]
14. Liao, L.-H.; Zheng, X.-F.; Kang, Y.-L.; Liu, W.; Yan, Y.; Mo, Z.-Y. Crystallographic texture and earing behavior analysis for different second cold reductions of double-reduction tinplate. *Int. J. Miner. Metall. Mater.* **2018**, *25*, 652–662. [[CrossRef](#)]
15. Xie, Q.-G.; Wang, Q.-L.; Luo, H.-W. Texture evolution of semi-processed non-oriented silicon steel with temper rolling. *Int. J. Miner. Metall. Mater.* **2009**, *31*, 855–866.
16. Meng, X.-C.; Luo, T.-L.; Shi, B.-H. Evolution rules of microstructure and property of sheets in CSP-CDCM-BA process. *J. Iron Steel Res.* **2007**, *19*, 40–44.
17. Radosław, W.; Olgierd, G.; Anna, K.; Mieczysław, K. Friction welding of tungsten heavy alloy with aluminium alloy. *J. Mater. Process. Technol.* **2017**, *246*, 42–55.



© 2019 by the authors. Licensee MDPI, Basel, Switzerland. This article is an open access article distributed under the terms and conditions of the Creative Commons Attribution (CC BY) license (<http://creativecommons.org/licenses/by/4.0/>).